Hindawi
Adsorption Science & Technology
Volume 2022, Article ID 8055615, 13 pages
https://doi.org/10.1155/2022/8055615

Research Article

Graphene Oxide/Fe_3O_4/Chitosan–Coated Nonwoven Polyester Fabric Extracted from Disposable Face Mask for Enhanced Efficiency of Organic Dye Adsorption

Hoang V. Tran, Nhan T. Hoang, Thu D. Le, Luyen T. Tran, and Hue T. M. Dang

School of Chemical Engineering, Hanoi University of Science and Technology, 1 Dai Co Viet Road, Hanoi, Vietnam

Correspondence should be addressed to Hoang V. Tran; hoang.tranvinh@hust.edu.vn and Thu D. Le; thu.ledieu@hust.edu.vn

Received 3 November 2021; Revised 9 December 2021; Accepted 23 December 2021; Published 25 January 2022

Academic Editor: Thi Ngoc Mai Pham

Owing to the COVID-19 pandemic, huge amounts of disposable face masks have been manufactured and used, and these discarded face masks have to be treated. In this study, we propose a simple approach for reusing the nonwoven polyester fabric (NWPF) from disposable face masks. In this approach, NWPF is utilized as a supporter for coating of a layer of graphene oxide/Fe_3O_4/chitosan (GFC) to form a GFC/NWPF adsorbent at room temperature via a simple spray coating method that does not require any solvent. The specific properties of GFC, NWPF, and the GFC/NWPF adsorbent were analysed via X-ray diffraction, transmission electron microscopy, ultraviolet–visible spectroscopy, vibrating sample magnetometry, and field-emission scanning electron microscopy. Results showed that the presence of NWPF enhanced the adsorption capacity of GFC towards organic dyes. At high concentrations of the organic dyes, the adsorption efficiency of the GFC/NWPF adsorbent to the dyes reached 100% within 24 h. The adsorption capacity (q_{max}) of the GFC/NWPF adsorbent to methylene blue, methyl orange, Congo red, and moderacid red was 54.795, 87.489, 88.573, and 29.010 mg g^{-1}, respectively, which were considerably higher than that of bulk GFC (39.308, 82.304, 52.910, and 21.249 mg g^{-1}, respectively).

1. Introduction

Organic dyes are widely used in many industries, such as textile, paper, rubber, plastic, leather, cosmetic, pharmaceutical, and food industries. However, the wastewater produced by these industries contains dyes and their products that contribute to water pollution, causing negative effects on humans and the environment, such as preventing the absorption of oxygen and sunlight and disrupting the respiration and growth of aquatic organisms. Furthermore, it causes adverse effects on the ability of microorganisms to decompose organic substances in wastewater [1–3]. Therefore, researchers have developed various wastewater treatment methods and have successfully applied them in removing colorants. These methods can be divided into three main categories, namely, biological, chemical, and physical methods [1]. Although physical and chemical methods, such as adsorption, photocatalysis, photocatalytic decomposition, membrane separation, ultrasonication, and wet air oxidation, are effective, they can only be applied when the concentration of the dissolved substances is sufficiently high. Moreover, some methods are expensive and still produce toxic by-products. By comparison, biological treatment methods include removing dyes via anaerobic and aerobic systems and fermenting activated sludge from filamentous fungi, yeasts, bacteria, and bacterial and fungal biomes. However, these methods also have disadvantages, such as long processing time and poor performance in removing dyes with a durable and a high-molecular polymeric structure. Moreover, the composition of these organic dyes in wastewater often harms the microorganism biomes/populations used in the sludge [4]. Among the aforementioned wastewater treatment methods, adsorption is considered one of the preeminent methods owing to its advantages, such as easy implementation, generation of nontoxic substances during the treatment process, high efficiency, and

low cost [5]. Furthermore, various adsorbent materials from traditional materials can used in adsorption, such as activated carbon, clay, agricultural by-products, banana peels, straw [5], rice husk [6], and red mud [7].

Graphene oxide (GO) and its composite-based adsorbents are excellent in adsorbing organic compounds, including organic dyes, as well as heavy metal ions [8–14]. GO is notable for its simpler fabrication and easier dispersion in water than other materials [15, 16]. Accordingly, GO is easy to use with a high adsorption efficiency. Functional molecules are utilized to generate functional groups to improve the adsorption capacity of GO to heavy metal ions or organic dyes. Chitosan (CS) molecule has several functional groups, such as primary –OH, secondary –OH, and $-NH_2$ groups. In these groups, the O and N atoms still have undivided electron pairs, making them the chemically active centres of CS. These groups are considered nucleophilic reagents and can participate in several specialized chemical responses [17] or complexed with almost all heavy metals and transition metals to help separate heavy metals from aqueous media easily [18]. Recently, Fe_3O_4 nanoparticles have been utilized to generate the magnetic property for adsorbents, thereby allowing them to be recovered and reused. In additions, the presence of Fe_3O_4 nanoparticles can improve the porosity of adsorbents [1, 2, 19, 20]. Therefore, GO/Fe_3O_4/CS (GFC) materials have excellent adsorption and recovery and regeneration abilities [21–23]. Hence, they are applied in the removal of organic dyes [2] and heavy metal ions [20].

Nonwoven fabric (NWPFs) is widely used in the production of medical disposable face masks and clothes [24–27]. NWPF can be combined with nanomaterials to enhance their properties, such as antibacterial, waterproof, and fireproof properties [28, 29]. The COVID-19 pandemic has necessitated the manufacturing and use of huge amounts of disposable face masks, and these discarded masks have to be treated [26]. Several recent reports have proposed using the NWPF extracted from discarded face masks and clothes as an adsorbent for the clean-up of waters polluted with petroleum and oil products [30], as a support of photocatalysts [31–33] or as a reinforcement of cement composites [27].

In this study, we propose a new approach for reusing NWPF. In this approach, NWPF is extracted from discarded disposable face masks as a support of a GFC nanocomposite adsorbent. The GFC/NWPF absorbent is fabricated by coating GFC onto NWPF via a simple and solvent-free spray coating method at room temperature (RT). Results showed that the presence of NWPF enhanced the adsorption capacity of the GFC absorbent to various organic dyes. Therefore, the GFC/NWPF absorbent will not only improve the adsorption capacity of GFC but also contribute to the efficient reuse of NWPF.

2. Experimental

2.1. Chemicals and Reagents. Graphite (99 wt.%, $d = 60 - 120\,\mu m$) was purchased from Vietnam Graphite Group (Vietnam). Sulfuric acid (H_2SO_4, 98 wt.%, AR), sodium nitrate ($NaNO_3$, AR), potassium permanganate ($KMnO_4$, AR), iron (III) chloride hexahydrate ($FeCl_3.6H_2O$, AR), iron (II) sulfide heptahydrate ($FeSO_4.7H_2O$, AR), sodium hydroxide (NaOH, 99 wt.%, AR), glacial acetic acid (CH_3COOH, 99 wt.%, AR), and hydrogen peroxide (H_2O_2, 33 wt.%, AR) were bought from Xilong Chemical Company (China). Methylene blue (MB), methyl orange (MO), Congo red (CR), and moderacid red (RS) were procured from Van Minh Chemical Company (Vietnam).

GO was prepared from graphite flakes following Hummer's method as described in previous reports [2, 20, 34, 35]. The GO product obtained was characterized via X-ray diffraction (XRD), scanning electron microscopy (SEM), and transmission electron microscopy (TEM) (Fig. SI.1). CS was prepared from shrimp shells in our laboratory in accordance with a previously published procedure [36]. The deacetylation degree (DD%) of CS was 85.0%; its average molecular weight (M_w) was 32.8 kDa. A 10 mg mL^{-1} CS solution was prepared by dissolving 5 g of CS in 500 mL of 1% (*v*/*v*) acetic acid solution and stirring overnight at RT to obtain a homogeneous and colorless solution. Fe_3O_4 nanoparticles were prepared by coprecipitating a mixture of iron (III) chloride hexahydrate and iron (II) sulfide heptahydrate at the molar ratio of 2 : 1 [2, 20, 34]. NWPF was extracted from discarded disposable face masks, washed with soap, sonicated with 95% (*v*/*v*) ethanol for 5 min, and dried at 80°C.

2.2. Preparation of the GFC/NWPF Absorbent. The GFC/NWPF absorbent was manufactured by coating a layer of GFC ink onto NWPF via a simple spray coating method. The GFC ink was prepared by mixing 0.22 g GO, 0.85 g Fe_3O_4, and 0.36 g CS. Afterwards, the mixture was dissolved in 100 mL 1 wt.% acetic solution and 0.5 mL glycerol by using a homogenizer under ultrasonic conditions for 30 min to obtain a black homogeneous ink of the GFC nanocomposite. The GFC ink was spray-coated onto the NWPF at RT. Finally, the NWPF was dried at 60°C for 2 h. This process was repeated five more times to increase the thickness of the coating. Finally, the NWPF was soaked in 1 M NaOH solution overnight, washed until it reached neutral pH, and dried at 80°C for 24 h to obtain the GFC/NWPF absorbent. Subsequently, the GFC/NWPF absorbent was cut into 1 cm × 1 cm samples for later use. The process of preparing the GFC/NWPF absorbent is illustrated in Scheme 1.

2.3. Adsorption Procedures. A piece of 1 cm × 1 cm GFC/NWPF sample (each sample contained 1.49 mg of the GFC powder) was immersed in 10 mL of an organic dye solution (MB, MO, CR, or RS). The mixture was incubated at various contact times at different temperatures. The pH of each solution was adjusted from 2 to 10 by adding 0.1 M HCl and 0.1 M NaOH solutions. The concentration of dye residues in the solution after the adsorption process was measured via UV-Vis spectrometry and by using suitable calibration curves (Figs. SI.3–SI.6). The adsorption capacity of the GFC/NWPF absorbent to the organic dyes was compared with that of bulk GFC by using 0.0194 g of the GFC powder instead of the GFC/NWPF sample. The dye removal

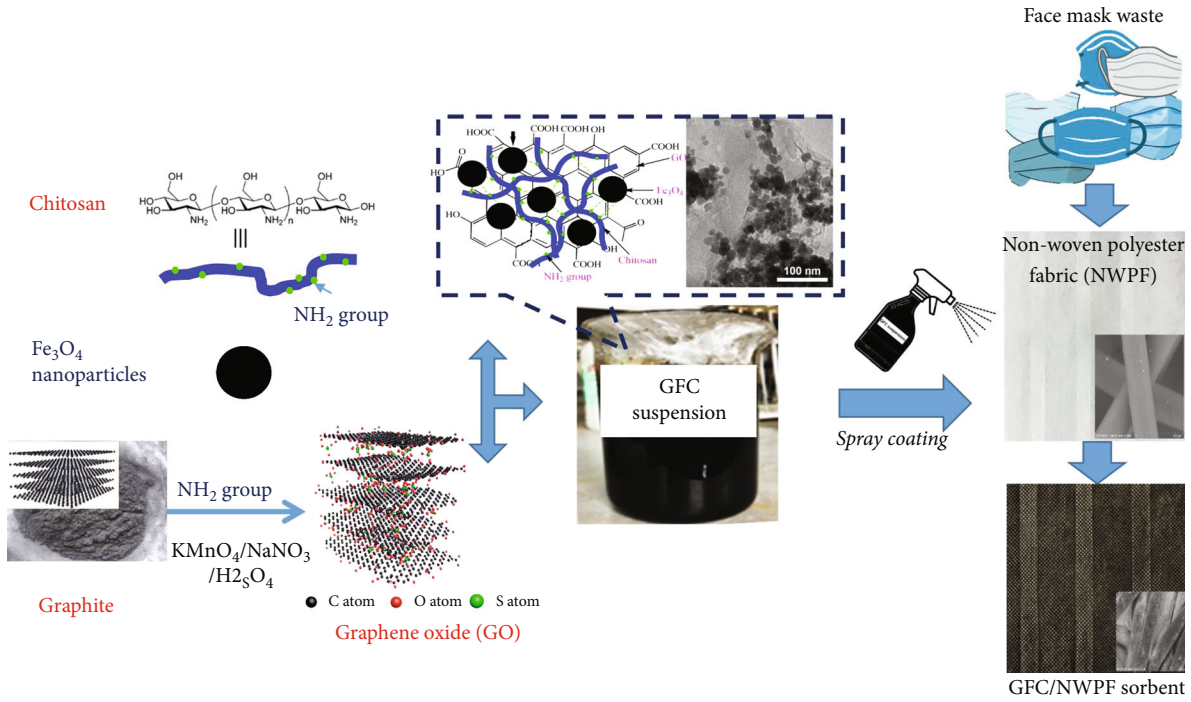

Scheme 1: The process of fabricating a new adsorbent by coating graphene oxide/Fe_3O_4/chitosan (GFC) coated onto nonwoven polyester fabric (NWPF) extracted from discarded disposable face masks.

efficiency of each composition in the composite was determined by testing various NWPF samples (Table 1). Dye removal efficiency (R, %) was calculated using the following equation (1):

$$R(\%) = \left(\frac{C_o - C_e}{C_o}\right) \times 100. \quad (1)$$

The amount of dye uptake by the GFC absorbent (q_e, $mg.g^{-1}$) was calculated as follows (equation (2)):

$$q_e = \frac{C_0 - C_e}{m_a}. \quad (2)$$

The Langmuir equation (3) and the Freundlich equation (4) isotherms were linearized into the following forms:

$$\frac{C_e}{q_e} = \frac{1}{K_L \times q_{max}} + \frac{1}{q_{max}} \times C_e, \quad (3)$$

$$\log q_e = \log K_F + \frac{1}{n} \times \log C_e, \quad (4)$$

where C_0 and C_e ($mg\,L^{-1}$) are the initial and equilibrium concentrations of organic dyes in solution, respectively; m_a is the mass of GFC ($g\,L^{-1}$); q_e and q_{max} are the equilibrium organic dye concentration on the adsorbent and the maximum adsorption capacity of the adsorbent ($mg\,g^{-1}$), respectively; K_L is the Langmuir constant ($L\,mg^{-1}$), which is related to the free energy of adsorption; K_F is the Freundlich constant ($L\,g^{-1}$); and n (dimensionless) is the heterogeneity factor.

2.4. Characterization and Methods. The XRD patterns of each GFC sample were obtained at RT by using a D8 Advance diffractometer (Bruker ASX) with CuKα radiation ($\lambda = 1.5406$ Å) within the range of $2\theta = 10 - 60°$ at a scanning rate of $0.02\,s^{-1}$. The morphology of the GFC nanocomposite and the GFC/NWPF samples was analysed via TEM (JEOL) at 100 kV × 200,000 magnification and FE-SEM (Hitachi S-4500), respectively. The magnetic behaviours of the samples were measured via vibrating sample magnetometry (VSM 880, DMS/ADE Technologies, USA) at fields ranging from −10 kOe to 10 kOe at 25°C with an accuracy of 10^{-5} emu. The concentration of organic dye residues in solution after the adsorption process was determined via UV-Vis spectrometry by establishing their calibration curves at the concentrations of 0.625, 1.25, 2.5, 5, 10, and 20 $mg\,L^{-1}$. Moreover, the calibration curves were established at pH 4, 5, 7, and 9. Afterwards, the spectra of these solutions were measured via UV-Vis spectrometry by using an Agilent 8453 UV-Vis spectrophotometer system within the wavelength range of 200–1200 nm. Subsequently, their optical density (OD) at the maximum adsorption was used to establish the calibration curves (OD vs. $C_{mg/L}$). The UV-Vis spectra and calibration curves are shown in the supporting information (SI) from Figs. SI.3 to SI.6.

3. Results and Discussion

3.1. Characterization of GFCs. The Fe_3O_4 nanoparticles agglomerated quite strongly because of their large specific surface energy; thus, the nanoparticles tended to agglomerate to reduce the surface energy (Figure 1(a)). The thickness of GO sheets was thin, only over 5 μm in size (Figure 1(b)).

Table 1: Removal efficiency (R%) of MB and MO by various coated NWPF samples at different pH levels.

Sample codes		M2	M3	M4	M5	M6	M7	M8	M9
Compositions	NWPFs	+[(a)]	+	+	+	+	+	+	+
	GO	—[(b)]	+	—	—	+	+	—	+
	CS	—	—	+	—	—	+	+	+
	Fe_3O_4	—	—	—	+	+	—	+	+
Acidic medium	R%[(c)] for MB	31.71	103.70	31.08	26.71	34.68	31.65	25.64	27.04
	R% for MO	4.55	34.65	31.48	14.95	26.07	27.97	57.01	53.51
Neutral medium	R% for MB	29.20	101.32	25.78	35.69	91.54	35.08	31.66	40.33
	R% for MO	4.58	20.73	17.78	6.73	14.67	6.68	9.64	8.19
Basic medium	R% for MB	35.08	105.37	39.78	39.78	99.25	99.82	46.63	86.66
	R% for MO	6.59	17.95	8.49	7.15	13.67	10.99	6.89	7.59

[(a)]Presence; [(b)]absence; [(c)]removal efficiency (R%).

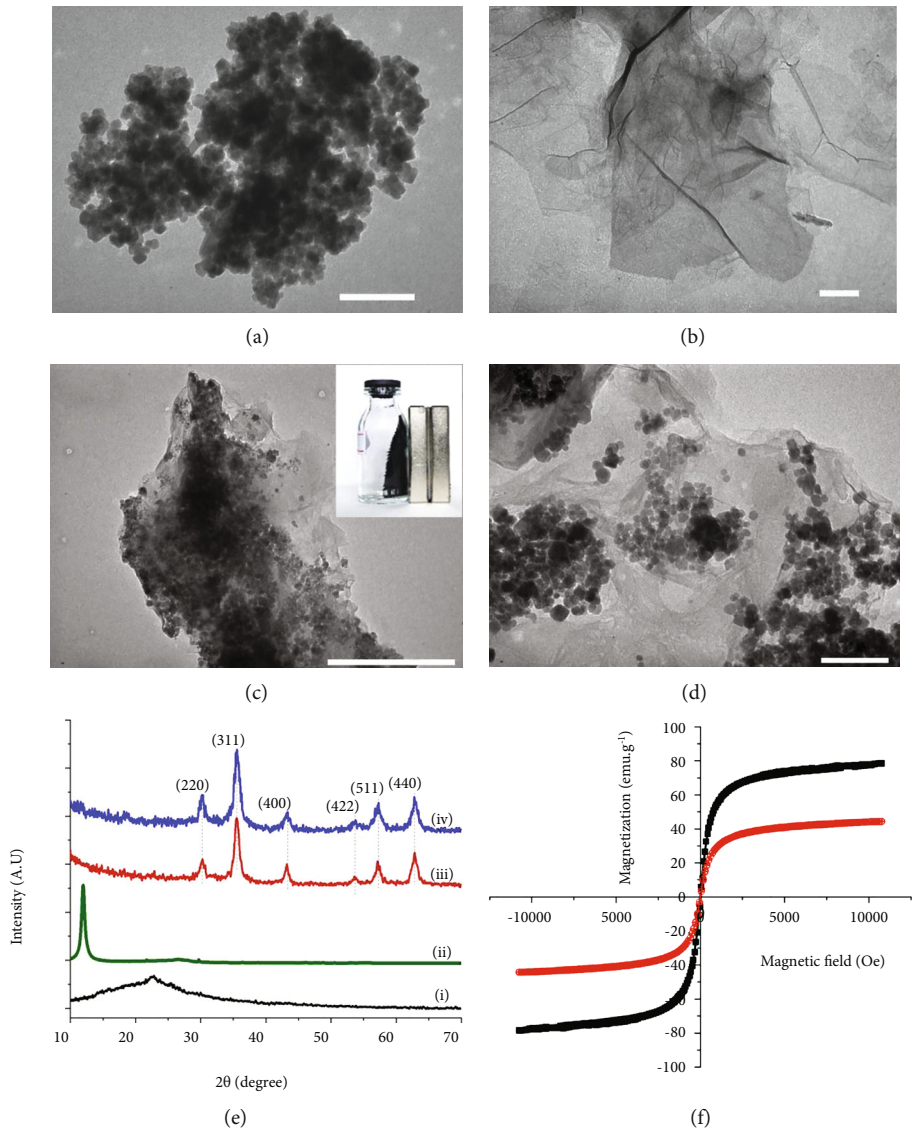

Figure 1: (a–d) TEM images of (a) Fe_3O_4 nanoparticles, (b) GO, and (c, d) GO/Fe_3O_4/CS (GFC) nanocomposite (inset: magnetic property of GFC nanocomposite); (d) XRD patterns of (i) CS, (ii) GO, (iii) Fe_3O_4, and (iv) GO/Fe_3O_4/CS; (f) VSM of (i) Fe_3O_4 and (ii) GO/Fe_3O_4/CS.

Spherical ferromagnetic particles of a fairly uniform size with an average diameter of about 30 nm scattered on the surfaces of GO and CS attached onto the thin GO sheets (Figures 1(c) and 1(d)). These spherical particles helped the Fe_3O_4 particles to attach onto the GO layer tightly. TEM results indicated that the GFC materials were successfully synthesized. No obvious peak could be observed from the XRD spectrum of CS (Figure 1(e), curve (i)). By contrast, a strong intensity peak (001) at $2\theta = 11.90^\circ$ could be observed from the XRD spectrum of GO (Figure 1(e), curve (ii)). The peak (002) of graphite at $2\theta = 27^\circ$ disappeared (Fig. SI.1b), indicating that GO was successfully synthesized. These results were similar to those of a previous study [37]. Both the XRD spectra of Fe_3O_4 (Figure 1(e), curve (iii)) and GO/Fe_3O_4/CS (Figure 1(e), curve (iv)) indicated that the synthesized Fe_3O_4 material was a single phase and had a low diffraction baseline, suggesting a complete crystalline phase. In the XRD spectrum of bare Fe_3O_4 nanoparticles (Figure 1(e), curve (iii)), six diffraction peaks appeared at 30.10°, 35.40°, 43.10°, 53.40°, 57.00°, and 62.50°, which corresponded to the (220), (311), (400), (422), (511), and (440) peaks of Fe_3O_4 (JCPDS File, PDF No. 65–3107) [11, 13, 22, 23], thereby confirming the formation of the magnetic spinel nanocrystal phase of Fe_3O_4. Comparing with that of pure Fe_3O_4, the diffraction spectrum of the GO/Fe_3O_4/CS sample retained the peaks of Fe_3O_4. Thus, CS and GO coatings did not affect the phase change in Fe_3O_4. The extension line in the figure was evaluated using the Debye–Scherrer equation, which describes the relationship between the width in XRD spectrum and particle size, as follows: $d = (k\lambda/\beta cos\,\theta)$, where d is the thickness of the crystal, $k = 0.89$ (the Debye–Scherrer constant), $\lambda = 0.15406$ nm (X-ray wavelength), β is the width at half-height of the peak, and θ is the Bragg angle. The average crystal size of Fe_3O_4 in the bare Fe_3O_4 sample was 30 nm, whereas that of the calculated sample was 35 nm. This result was consistent with the TEM images (Figure 1). The magnetic property of GFC was tested with magnets. GFC exhibited strong interactions with the magnets (Figure 1(c), inserted figure). Theoretically, CS and GO are nonmagnetic. Thus, the magnetic property of the GO/Fe_3O_4/CS material was due to the presence of Fe_3O_4. The magnetization curves of the Fe_3O_4 and GO/Fe_3O_4/CS samples (Figure 1(f)) demonstrated that they have superparamagnetic properties. The magnetic saturation (M_s) of the Fe_3O_4 sample was ~80 emu g^{-1} (Figure 1(f), curve (i)), whereas that of the GFC sample was ~40 emu g^{-1} (Figure 1(f), curve (ii)). Therefore, the coverage of CS and GO on the Fe_3O_4 particles substantially reduced the magnetization. As results show, the Ms of the GFC sample was still high (40 emu g^{-1}); thus, it was able to coat NWPF and endowed GFC/NWPF with magnetic properties to separate the GFC/NWPF after absorption process using an external magnet for the regeneration and circulation. According to the FTIR spectra of CS and GFC (Fig. SI.2), the main specific groups in CS included an adsorption at 3578 cm^{-1}, which was attributed to the stretching vibration of the O–H group; a band at approximately 2881 cm^{-1}, which was ascribed to the stretching vibration of C–H; and characteristic adsorption bands at 1674 and 1589 cm^{-1}, which corresponded to C=O stretching and N–H blending in the amide groups, respectively [38–41]. However, in the FTIR spectrum of GFC, these specific bands of amide groups shifted to 1597, 1516, and 1394 cm^{-1}, respectively. The presence of amine and amide groups on the GFC surface plays an important role in organic dye removal [38–43].

3.2. Characterization of NWPF and the GFC/NWPF Absorbent. The GO/Fe_3O_4/CS materials were coated onto NWPF via a simple spray coating method. Five coats were applied to create a sufficiently thick and even coating. The mass density (d, g cm^{-2}) of the GFC coated onto the 1 cm^2 NWPF samples was calculated as follows:

$$d = \frac{m_{\mathrm{GFC(g)}}}{S_{\mathrm{NWPF}}(\mathrm{cm}^2)}, \tag{5}$$

where m_{GFC} is the amount of GFC used for coating (g) and S_{NWPF} is the total area of NWPF covered (cm^2). In this experiment, $m_{\mathrm{GFC}} = 0.22$ g of GO + 0.85 g of Fe_3O_4 + 0.36 g of CS (=1.43 g) and $S_{\mathrm{NWPFs}} = 959$ cm^2; hence, $d = 1.49$ mg GFC cm^{-2}.

SEM images of NWPF and the GFC/NWPF absorbent are shown in Figure 2. The polyester fibres in NWPF were slippery and even, their surface was smooth, and it consisted of overlapping nonwoven fibres that were pressed by heat (Figures 2(a), 2(c), 2(e), and 2(g)). By comparison, after GFC was coated onto NWPF, the surface of the polyester fibres in the GFC/NWPF absorbent became rough and rugged (Figures 2(b), 2(d), 2(f), and 2(h)), and the coating cracked at some points (Figures 2(d), 2(f), and 2(h)). Moreover, the size of the fibres considerably increased. By contrast, the GO sheets (Figures 2(d) and 2(h)) and the Fe_3O_4 nanoparticles (Figure 2(h), inserted figure) became rumpled. These results indicated that GFC was successfully coated onto the surface of NWPF via the simple spray coating method adopted herein. Thus, this method can be employed in fabricating GFC/NWPF absorbents on a large scale.

3.3. Adsorption of Organic Dyes on GFC and GFC/NWPF Absorbents

3.3.1. Optimization of Adsorption Conditions. The adsorption conditions were optimized including the pH and compositions of the GFC/NWPF adsorbent to enhance its adsorption of organic dyes. Eight coated NWPF samples with different compositions were prepared (Table 1). Their ability to absorb MB (a cationic dye) and MO (an anionic dye) was evaluated at different pH 5, 7, and 9. Organic dyes can be classified into three types: cationic organic dyes with a positive charge, anionic organic dyes with a negative charge, and nonionic organic dyes with no charge. Therefore, the adsorption of the dyes onto the adsorbents can be achieved via electrostatic interactions between dye ions and groups of opposite charge as the functional groups on an adsorbent's surface. However, this classification is only relative because an organic dye can be an anionic or a cationic dye depending on the environment (pH) (Table 2). The surface of the GFC/NWPF absorbent had abundant amine groups

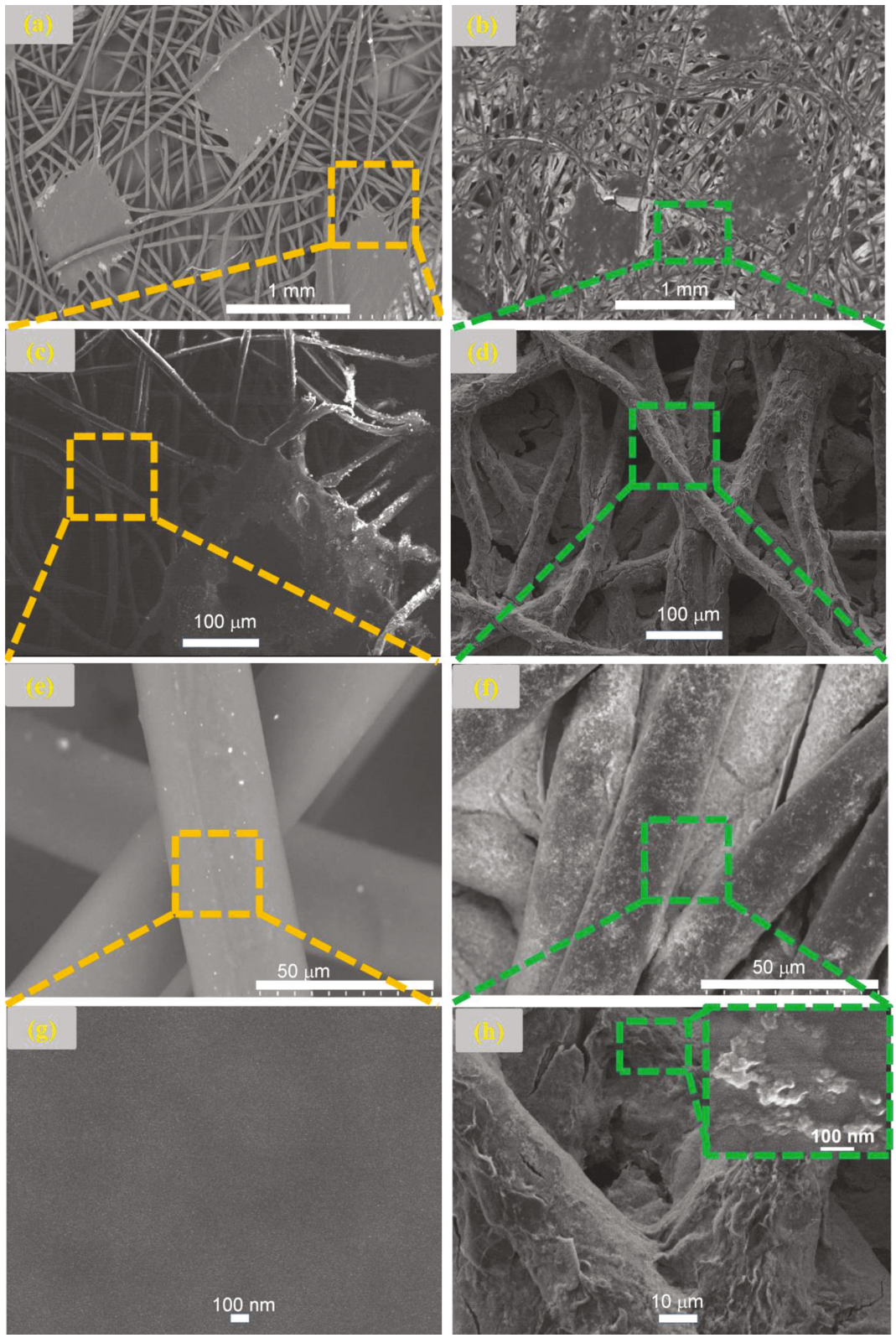

Figure 2: SEM and FESEM images of (a, c, e, g) NWPF and (b, d, f, h) GFCs/NWPF.

($-NH_2$) from CS and –COOH. The –OH groups of GO are suitable for nonionic dyes when they are in a neutral environment. In an acidic environment, these groups will become $-NH_3^{\oplus}$, $-COOH_2^{\oplus}$, and $-OH_2^{\oplus}$; thus, they are suitable for absorbing MO, RS, and CR. Moreover, in an alkaline environment, these functional groups will become $-NH_2$, $-COO^{\ominus}$, and $-O^{\ominus}$, respectively, which are suitable for absorbing MB [1, 2, 35, 44–47].

Table 2: Comparison of the adsorption capacity of the adsorbents assessed herein.

Dyes	Conditions	Adsorbents	Adsorption model		Comparison of q_{max} ($mg\,g^{-1}$) with that of other adsorbents
			Langmuir	Freundlich	
Methylene blue (MB)	pH = 9, RT, $T = 2\,h$	GFC/NWPFs	$C_e/q_e = 0.018 * C_e + 0.096$ $R^2 = 0.980$ and $q_{max} = 54.795\,mg\,g^{-1}$	$\log q_e = 0.108 * \log C_e + 1.245$ $R^2 = 0.927$	GO–β-cyclodextrin–chitosan@Fe_3O_4: $q_{max} = 84.32\,mg\,g^{-1}$ [52]; CS/Fe_3O_4/GO: $q_{max} = 30.01\,mg\,g^{-1}$ [2]; Fe_3O_4/C core–shell structure: $q_{max} = 44.38\,mg\,g^{-1}$ [53]
		GFC	$C_e/q_e = 0.025 * C_e + 0.125$ $R^2 = 0.970$ and $q_{max} = 39.308\,mg\,g^{-1}$	$\log q_e = 0.193 * \log C_e + 1.245$ $R^2 = 0.742$	
Methyl Orange (MO)	pH = 4, RT, $T = 2\,h$	GFC/NWPF	$C_e/q_e = 0.011 * C_e + 0.401$ $R^2 = 0.9108$ and $q_{max} = 87.489\,mg\,g^{-1}$	$\log q_e = 0.736 * \log C_e + 0.550$ $R^2 = 0.990$	γ–Fe_2O_3/chitosan composite film: $q_{max} = 29.41\,mg\,g^{-1}$ [54]; amine/Fe_3O_4–resin composite: $q_{max} = 101\,mg\,g^{-1}$ [55]
		GFC	$C_e/q_e = 0.012 * C_e + 0.569$ $R^2 = 0.878$ and $q_{max} = 82.304\,mg\,g^{-1}$	$\log q_e = 0.753 * \log C_e + 0.411$ $R^2 = 0.978$	
Congo red (CR)	pH = 4, RT, $T = 2\,h$	GFC/NWPF	$C_e/q_e = 0.011 * C_e + 0.905$ $R^2 = 0.947$ and $q_{max} = 88.573\,mg\,g^{-1}$	$\log q_e = 0.725 * \log C_e + 0.310$ $R^2 = 0.994$	XG–g–PAM/SiO_2 nanocomposite: $q_{max} = 209.2\,mg\,g^{-1}$ [56]; spherical microparticles MgO–GO: $q_{max} = 227\,mg\,g^{-1}$ [57]
		GFC	$C_e/q_e = 0.019 * C_e + 0.212$ $R^2 = 0.945$ and $q_{max} = 52.910\,mg\,g^{-1}$	$\log q_e = 0.388 * \log C_e + 1.020$ $R^2 = 0.9342$	
Moderacid red (RS)	pH = 4, RT, $T = 2\,h$	GFC/NWPF	$C_e/q_e = 0.034 * C_e + 0.433$ $R^2 = 0.939$ and $q_{max} = 29.010\,mg\,g^{-1}$	$\log q_e = 0.548 * \log C_e + 0.545$ $R^2 = 0.963$	Fe_3O_4 nanoparticles and amine/Fe_3O_4–resin composite: $q_{max} = 40.2$ and $99.4\,mg\,g^{-1}$, respectively [55]; Fe_3O_4@GPTMS@P–Lys: $q_{max} = 134.7\,mg\,g^{-1}$ [58]
		GFC	$C_e/q_e = 0.047 * C_e + 0.902$ $R^2 = 0.899$ and $q_{max} = 21.249\,mg\,g^{-1}$	$\log q_e = 0.560 * \log C_e + 0.297$ $R^2 = 0.871$	

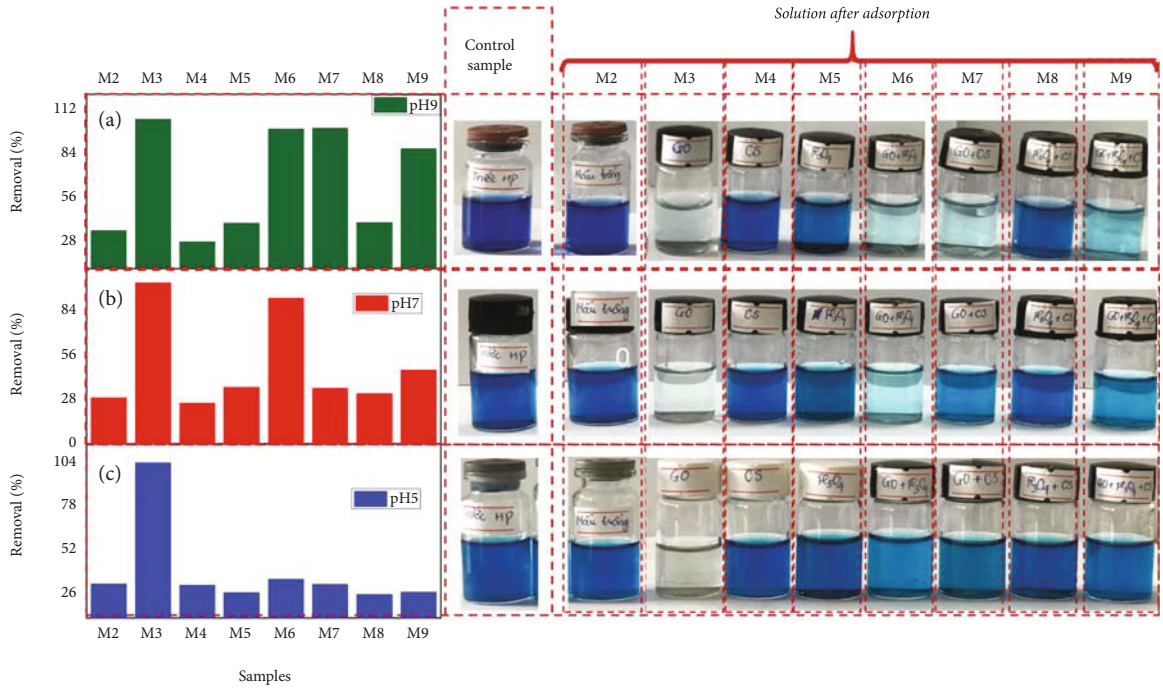

Figure 3: Effects of pH on MB adsorption onto the GFC/NWPF absorbent: (a) pH 5, (b) pH 7, and (c) pH 9 (inserted images: corresponding color of MB solutions before and after the adsorption process).

Figure 3(a) shows that GO/NWPF sample (coded M3) adsorbed MB very well for all medium with removal efficiency (R %) which was 100%. Besides, all adsorbents containing GO, i.e., GO/Fe_3O_4/NWPFs (coded M6), GO/CS/NWPFs (coded M7), and GFC/NWPFs (coded M9) samples, performed good adsorption MB in basic medium (pH 9) with the highest R % values that were obtained, which were 99%, 99%, and 86%, respectively. On the contrary, without GO, the R% values were low for MB adsorption on NWPFs (coded M2) or CS/NWPFs (coded M4), or Fe_3O_4/NWPFs (coded M5) or CS/Fe_3O_4/NWPFs (coded M8) samples. Figure 3 also shows that the R% values were higher than that for neutral medium (pH 7) (Figure 3(b)) or acidic medium (pH 5) (Figure 3(c)). Obtained results imply that, for efficiency removal of MB in solution, the adsorption process should be carried out in alkaline medium, and GO presented in GO/CS/NWPFs played an important role towards MB removal.

In removing the anionic dye MO (Figure 4), the R% values for all samples were very low (<20%) at pH 9 (Figure 4(a)) and 7 (Figure 4(b)). However, in an acidic medium (pH 5), their R% values were higher (Figure 4(c)). The R% value for MO adsorption onto the M6 (GO/Fe_3O_4/NWPF) and M7 (GO/CS/NWPF) samples was 26%–27%. Furthermore, the R% value was 31%–35% for the M3 (GO/NWPF) and M4 (CS/NWPFs) samples and 53%–58% for the M8 (CS/Fe_3O_4/NWPF) and M9 (GFC/NWPFs) samples. The R% values were very small for MO adsorption onto the M2 (NWPF) (4%) and M5 (Fe_3O_4/NWPF) (14%) samples. These data indicated that MO removal was more difficult to achieve than MB removal in the systems proposed herein. This difference can be attributed to the structure of MO: it has two oppositely charged centres, namely, a positively charged centre from $-N^{\oplus}(CH_3)$ and a negatively charged centre from $-SO_3^{\ominus}$. Hence, both CS (which contains $-NH_3^{\oplus}$) and GO (which contains $-COO^{\ominus}$ and $-OH_2^{\oplus}$) play an important role in MO adsorption via electrostatic interactions. Therefore, the M9 sample (GFC/NWPF, which contained both CS and GO components) was able to satisfactorily remove anionic dyes (including MO, RS, and CR) in the acidic medium (pH 5). The attractive forces required to adsorb dye molecules (MB, MO, CR, and RS) onto the surface of the GFC/NWPF adsorbent were not only attributed to electrostatic interactions; it also included due to $\pi-\pi$ stacking interactions, i.e., the strong interaction between the π-conjugated electron systems of MB, MO, CR, and RS molecules (Table SI.1) with the π-conjugated electrons of GO via $\pi-\pi$ stacking interactions [1, 2, 31, 32, 42, 43, 48–51]. Accordingly, increasing the content of GO improved the adsorption capacity (q_{max}). However, increasing the content of GO should be limited owing to economic (the price of the adsorbent will increase) and technical (the release of GO from the adsorbent into the solution should be avoided) considerations.

The effects of the absorbents' components on dye adsorption capacity were evaluated. Five coated NWPF samples (S1, S2, S3, S4, and S5) were fabricated and tested for MB adsorption (Figure 5). Figure 5(a) shows the UV-Vis spectrum of the MB solution after adsorption by GFC powder for 2 h at RT and pH 9. The S1, S2, S3, S4, and S5 samples had compositions of GO, Fe_3O_4, and CS by mass ($m_{GO}:m_{Fe3O4}:m_{CS}$) of 50:40:10, 50:10:40, 0:50:50, 10:60:30, and 10:40:50, respectively. The adsorption efficiency of each sample was very different: the samples with

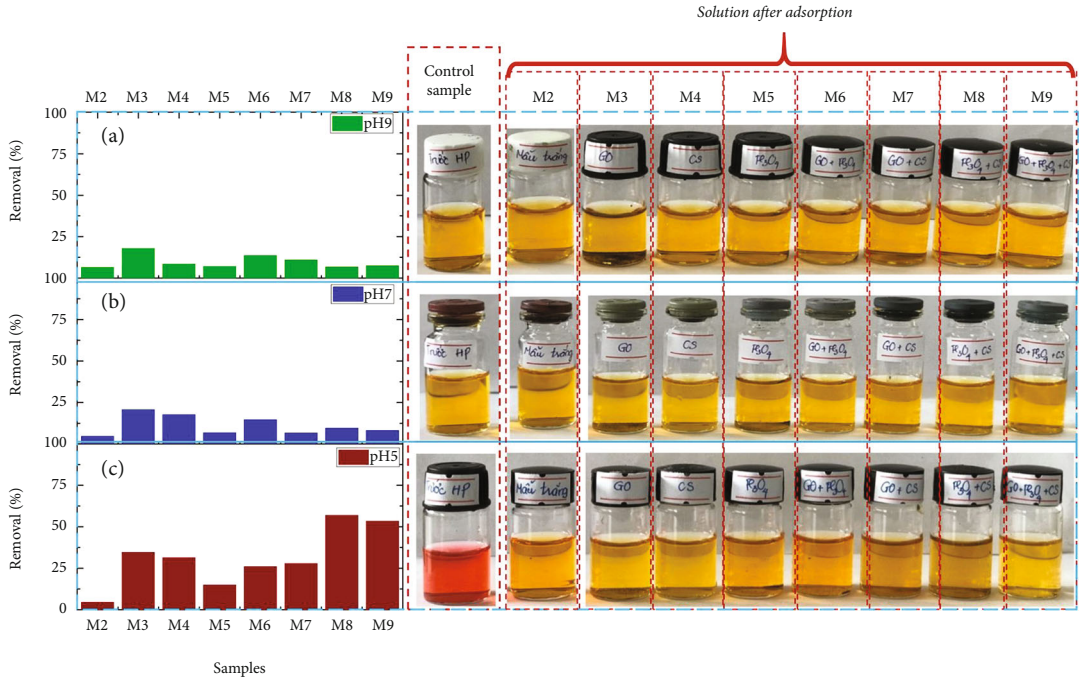

FIGURE 4: Effects of pH on MO adsorption onto the GFC/NWPF absorbent: (a) pH 5, (b) pH 7, and (c) pH 9 (inserted images: corresponding color of MO solutions before and after the adsorption process).

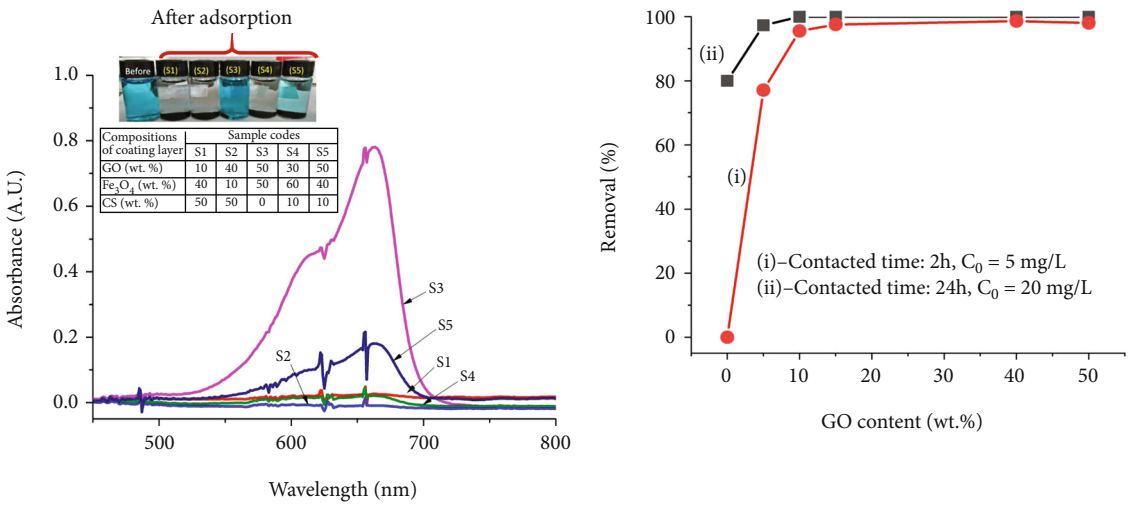

FIGURE 5: (a) UV-Vis spectra of samples after adsorption of MB solutions (inserted images are the colors of the MB solutions before and after adsorption onto GO/Fe_3O_4/CS [percent by weight, wt.%]: S1 [50 : 40 : 10], S2 [50 : 10 : 40], S3 [0 : 50 : 50], S4 [10 : 60 : 30], and S5 [10 : 40 : 50]). (b) Influence of GO content on MB removal at various times and (i) $C_0 = 5\,\text{mg}\,\text{L}^{-1}$ and (ii) $C_0 = 20\,\text{mg}\,\text{L}^{-1}$.

high GO content (S1 and S2) had very large adsorption capacity (R% was 98.03% and 98.0%, respectively). When doped with Fe_3O_4 and CS, the efficiency of the samples with low GO content substantially increased. The S4 sample had only 10% GO, but its adsorption efficiency was large (R% was 95.55%). However, when excessive amounts of CS were added, the R% value dramatically decreased to 77.08% in the S5 sample (containing 50 wt.% CS) and even down to 0% in the S3 sample (containing 0 wt.% GO and 50 wt.% CS). Adding excessive amounts of CS considerably reduced the porosity of the materials. Therefore, GO should be added as much as possible while limiting the content of CS to 10 wt.%–40 wt.%. However, the production costs of GO are high. Thus, instead of adding 40 wt.%–50 wt.% of GO to remove MB at $R\% > 90\%$ in 2 h, $R\% > 90\%$ can still be achieved when 10 wt.% of GO is added by simply extending the adsorption time to 24 h (Figure 5(b)). When the content of GO was increased from 20 wt.% to 50 wt.%, the value of

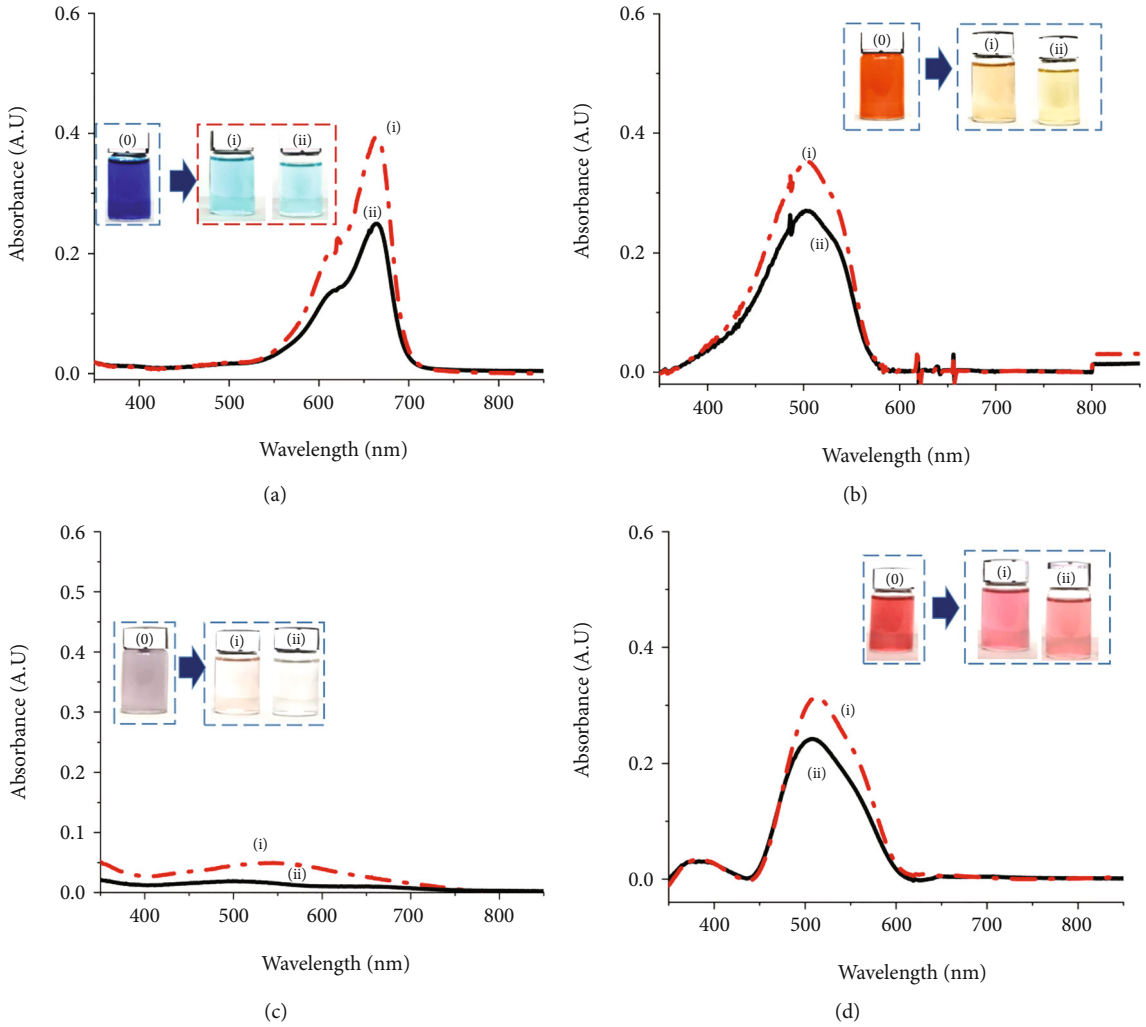

FIGURE 6: UV-Vis spectra of colorant solutions after adsorption of (a) MB, (b) MO, (c) CR, and (d) RS onto (i) GFC (red dot–dash) and (ii) GFC/NWPF (black solid) (inserted image: color of colorant solutions before and after adsorption).

R% did not increase (Figure 5(b)). Therefore, the addition of 10 wt.% of GO is the best level that achieves the optimum technical–economic efficiency.

3.3.2. Comparison of the Adsorption of MB, MO, CR, and RS onto the GFC/NWPF Absorbent and Bulk GFC. The adsorption efficiency of bulk GFC was compared with that of the GFC/NWPF absorbent under the same conditions with the same amount of GFC converted. Both the powder and coated samples achieved very good adsorption efficiency for MB, MO, CR, and RS, and the color of the solutions was almost completely eliminated (Figure 6). In all cases, the GFC/NWPF samples seemed to remove the colorants better than the GFC: *R*% was 97.98% and 96.11% for MB (Figure 6(a)), 96.25% and 94.86% for MO (Figure 6(b)), 97.15% and 84.47% for CR (Figure 6(c)), and 83.68% and 78.22% for RS (Figure 6(d)), respectively. Differences in color could also be observed with the naked eye (pictures inserted in the figures). This result confirmed that coating GFC is necessary to improve its adsorption performance.

3.3.3. Adsorption Isotherms of MB, MO, CR, and RS onto the GFCs/NWPF Absorbent. The adsorption isotherms of MB, MO, RS, and CR on both bulk GFC and the GFC/NWPF absorbent were built according to the Langmuir and Freundlich models by using equations (3) and (4) (Table 2 and Figs. SI.7–SI.10). On the basis of the correlation coefficient (R^2), the process by which the organic dyes absorb on both bulk GFC and the GFC/NWPF absorbent was more consistent with the Langmuir model than with the Freundlich model. The maximum adsorption capacity (q_{max}) of the GFC/NWPF absorbent for all organic dyes was higher than that of bulk GFC (Table 2). Results indicated that the presence of NWPF enhanced q_{max}. Compared the absorption efficiency for MB, MO, RS, and CR of the various reported materials, the q_{max} values for MB or MO of the developed hybrid materials herein including bulk GFC and the GFC/NWPF adsorbents are competitive and lower for RS and CR adsorption (Table 2). However, an advantage of the developed bulk GFC and GFC/NWPF adsorbents is they can be made via a simple synthesis process.

4. Conclusions

NWPF was extracted from discarded disposable face masks and used as a support to prepare a GFC nanocomposite-based adsorbent. GFC was successfully onto NWPF. The presence of NWPF enhanced the adsorption efficiency of GFC for the organic dyes MB, MO, CR, and RS. In all cases, the coating improved the adsorption performance of the GFC materials. The adsorption efficiency of the GFC/NWPF adsorbent for these organic dyes was higher than that of bulk GFC with the same mass. Obtained results demonstrated that the adsorption efficiency of the GFC/NWPF adsorbent was different for MB, MO, CR, and RS dyes and can be competitive to previously reported materials implying that the GFC/NWPF absorbent has a high application potential.

Data Availability

The data used to support the findings of this study are included within the article.

Conflicts of Interest

The authors declare that they have no conflict of interest.

Acknowledgments

This work was supported by the Vietnam Ministry of Education and Training (under project number B2020-BKA-15).

Supplementary Materials

Table IS.1: molecular structure and some specific properties of MB, MO, CR, and RS. Figure SI.1: characterizations of GO: (a) UV-Vis spectrum (inserted figure: digital photo of GO solution and GO flakes), (b) XRD, (c, d) SEM, (e) FE-SEM, and (f) TEM images. Figure SI.2: FT-IR spectra of (a) chitosan (CS) and (b) graphene oxide/Fe3O4/chitosan (GFC). Figure SI.3: right, UV-Vis spectra of MO solution at various MO concentrations and left, corresponding calibration curves for MO determination at various pH: (i) pH = 4, (ii) pH = 5, (iii) pH = 7, and (iv) pH = 9. Figure SI.4: right, UV-Vis spectra of MB solution at various MB concentrations and left, corresponding calibration curves for MB determination at various pH: (i) pH = 5, (ii) pH = 7, and (iii) pH = 9. Figure SI.5: (i) UV-Vis spectra of CR solution at various CR concentrations and (ii) corresponding calibration curves for CR determination at pH = 4. Figure SI.6: (i) UV-Vis spectra of RS solution at various RS concentrations and (ii) corresponding calibration curves for CR determination at pH = 4. Fig. SI.7: adsorption isotherm according to (a, c) Langmuir and (b, d) Freundlich models of MB on (a, b) GFCs/NWPFs and (c, d) bulk GFCs, respectively. Fig. SI.8: adsorption isotherm according to (a, c) Langmuir and (b, d) Freundlich models of MO on (a, b) GFCs/NWPFs and (c, d) bulk GFCs, respectively. Fig. SI.9: adsorption isotherm according to (a, c) Langmuir and (b, d) Freundlich models of CR on (a, b) GFCs/NWPFs and (c, d) bulk GFCs, respectively. Fig. SI.10: adsorption isotherm according to (a, c) Langmuir and (b, d) Freundlich models of RS on (a, b) GFCs/NWPFs and (c, d) bulk GFCs, respectively. *(Supplementary Materials)*

References

[1] H. V. Tran, L. T. Hoang, and C. D. Huynh, "An investigation on kinetic and thermodynamic parameters of methylene blue adsorption onto graphene-based nanocomposite," *Chemical Physics*, vol. 535, article 110793, 2020.

[2] H. V. Tran, L. T. Bui, T. T. Dinh, D. H. Le, C. D. Huynh, and A. X. Trinh, "Graphene oxide/Fe3O4/chitosan nanocomposite: a recoverable and recyclable adsorbent for organic dyes removal. Application to methylene blue," *Materials Research Express*, vol. 4, no. 3, 2017Article number 035701.

[3] S. Vallinayagam, K. Rajendran, S. K. Lakkaboyana et al., "Recent developments in magnetic nanoparticles and nanocomposites for wastewater treatment. Journal of Environmental," *Chemical Engineering*, vol. 9, no. 6, article 106553, 2021.

[4] C. Fernández, M. S. Larrechi, and M. P. Callao, "An analytical overview of processes for removing organic dyes from wastewater effluents," *TrAC Trends in Analytical Chemistry*, vol. 29, no. 10, pp. 1202–1211, 2010.

[5] W. Zhang, H. Li, X. Kan et al., "Adsorption of anionic dyes from aqueous solutions using chemically modified straw," *Bioresource Technology*, vol. 117, pp. 40–47, 2012.

[6] M. Ajmal, R. A. K. Rao, S. Anwar, J. Ahmad, and R. Ahmad, "Adsorption studies on rice husk: removal and recovery of Cd(II) from wastewater," *Bioresource Technology*, vol. 86, no. 2, pp. 147–149, 2003.

[7] H. Genç, J. C. Tjell, D. McConchie, and O. Schuiling, "Adsorption of arsenate from water using neutralized red mud," *Journal of Colloid and Interface Science*, vol. 264, no. 2, pp. 327–334, 2003.

[8] S. Debnath, A. Maity, and K. Pillay, "Impact of process parameters on removal of Congo red by graphene oxide from aqueous solution," *Journal of Environmental Chemical Engineering*, vol. 2, no. 1, pp. 260–272, 2014.

[9] W. Peng, H. Li, Y. Liu, and S. Song, "A review on heavy metal ions adsorption from water by graphene oxide and its composites," *Journal of Molecular Liquids*, vol. 230, pp. 496–504, 2017.

[10] D. Robati, B. Mirza, M. Rajabi et al., "Removal of hazardous dyes-BR 12 and methyl orange using graphene oxide as an adsorbent from aqueous phase," *Chemical Engineering Journal*, vol. 284, pp. 687–697, 2016.

[11] J.-S. Choi, L. P. Lingamdinne, J.-K. Yang, Y.-Y. Chang, and J. R. Koduru, "Fabrication of chitosan/graphene oxide-gadolinium nanorods as a novel nanocomposite for arsenic removal from aqueous solutions," *Journal of Molecular Liquids*, vol. 320, article 114410, 2020.

[12] D. J. Joshi, J. R. Koduru, N. I. Malek, C. M. Hussain, and S. K. Kailasa, "Surface modifications and analytical applications of graphene oxide: a review," *TrAC Trends in Analytical Chemistry*, vol. 144, article 116448, 2021.

[13] L. P. Lingamdinne, J. R. Koduru, and R. R. Karri, "A comprehensive review of applications of magnetic graphene oxide based nanocomposites for sustainable water purification," *Journal of Environmental Management*, vol. 231, pp. 622–634, 2019.

[14] L. P. Lingamdinne, J. R. Koduru, Y. Y. Chang, M. Naushad, and J. K. Yang, "Polyvinyl alcohol polymer functionalized

graphene oxide decorated with gadolinium oxide for sequestration of radionuclides from aqueous medium: Characterization, Mechanism, and Environmental Feasibility Studies," *Polymers*, vol. 13, no. 21, article 3835, 2021.

[15] D. R. Dreyer, S. Park, C. W. Bielawski, and R. S. Ruoff, "The chemistry of graphene oxide," *Chemical Society Reviews*, vol. 39, no. 1, pp. 228–240, 2010.

[16] J.-G. Yu, L.-Y. Yu, H. Yang et al., "Graphene nanosheets as novel adsorbents in adsorption, preconcentration and removal of gases, organic compounds and metal ions," *Science of the Total Environment*, vol. 502, pp. 70–79, 2015.

[17] K. Z. Elwakeel, "Environmental application of chitosan resins for the treatment of water and wastewater: a review," *Journal of Dispersion Science and Technology*, vol. 31, no. 3, pp. 273–288, 2010.

[18] P. Szymczyk, U. Filipkowska, T. Jóźwiak, and M. Kuczajowska-Zadrożna, *The use of chitin and chitosan for the removal of reactive black 5 dye*, Progress on Chemistry and Application of Chitin and Its Derivatives XX, 2015.

[19] H. V. Tran, L. T. Hoang, and H. T. T. Huyen, *Electrochemical Synthesis of Graphene from Waste Discharged Battery Electrodes and Its Applications to Preparation of Graphene/Fe3O4/Chitosan-Nanosorbent for Organic Dyes Removal*, Zeitschrift für anorganische und allgemeine Chemie, 2021.

[20] H. V. Tran, T. L. Tran, T. D. Le, T. D. Le, H. M. T. Nguyen, and L. T. Dang, "Graphene oxide enhanced adsorption capacity of chitosan/magnetite nanocomposite for Cr (VI) removal from aqueous solution," *Materials Research Express*, vol. 6, no. 2, article 025018, 2019.

[21] G. Sheng, Y. Li, X. Yang et al., "Efficient removal of arsenate by versatile magnetic graphene oxide composites," *RSC Advances*, vol. 2, no. 32, pp. 12400–12407, 2012.

[22] T. N. Nguyen, H. T. B. Pham, H. V. Tran, H. D. Vu, K. V. Nguyen, and L. D. Tran, "Magnetic chitosan nanoparticles for removal of Cr (VI) from aqueous solution," *Materials Science and Engineering: C*, vol. 33, no. 3, pp. 1214–1218, 2013.

[23] H. V. Tran, L. D. Tran, and T. N. Nguyen, "Preparation of chitosan/magnetite composite beads and their application for removal of Pb (II) and Ni (II) from aqueous solution," *Materials Science and Engineering: C*, vol. 30, no. 2, pp. 304–310, 2010.

[24] M. Elisabeth, "Covid-19: are cloth masks still effective? And other questions answered," *British Medical Journal*, vol. 372, article n432, 2021.

[25] N. Karim, S. Afroj, K. Lloyd et al., "Sustainable personal protective clothing for healthcare applications: a review," *ACS Nano*, vol. 14, no. 10, pp. 12313–12340, 2020.

[26] F. G. Torres and G. E. De-la-Torre, "Face mask waste generation and management during the COVID-19 pandemic: an overview and the Peruvian case," *Science of The Total Environment*, vol. 786, article 147628, 2021.

[27] P. Sadrolodabaee, J. Claramunt, M. Ardanuy, and A. de la Fuente, "A textile waste fiber-reinforced cement composite: comparison between short random fiber and textile reinforcement," *Materials*, vol. 14, article 3742, 2021.

[28] A. K. M. A. H. Asif and M. Z. Hasan, "Application of nanotechnology in modern textiles: a review," *International Journal of Current Engineering and Technology*, vol. 8, no. 2, pp. 227–231, 2014.

[29] M. J. Madou, *Manufacturing Techniques for Microfabrication and Nanotechnology*, CRC press, 2011.

[30] M. Neznakomova, S. Boteva, L. Tzankov, and M. Elhag, "Non-woven textile materials from waste fibers for cleanup of waters polluted with petroleum and oil products," *Earth Systems and Environment*, vol. 2, pp. 413–420, 2018.

[31] M. U. Dao, T. T. T. Nguyen, V. T. Le et al., "Non-woven polyester fabric-supported cuprous oxide/reduced graphene oxide nanocomposite for photocatalytic degradation of methylene blue," *Journal of Materials Science*, vol. 56, pp. 10353–10366, 2021.

[32] K. Huo, J. Wang, T. Zhuang et al., "Facile fabrication of recyclable and macroscopic D-g-C3N4/sodium alginates/non-woven fabric immobilized photocatalysts with enhanced photocatalytic activity and antibacterial performance," *Journal of Materials Science*, vol. 56, no. 31, pp. 17584–17600, 2021.

[33] G. Luo, Q. Yu, L. Yu, X. Wang, X. Hao, and J. Fu, "Preparation and characterization of platinum nanoparticles supported by non-woven fabric for formaldehyde decomposition," *Fibers and Polymers*, vol. 20, pp. 2099–2105, 2019.

[34] T. D. Le, L. T. Tran, H. T. M. Dang, H. T. T. Tran, and H. V. Tran, "Graphene oxide/polyvinyl alcohol/Fe3O4 nanocomposite: an efficient adsorbent for Co (II) ion removal," *Journal of Analytical Methods in Chemistry*, vol. 2021, Article ID 6670913, 2021.

[35] L. T. Tran, H. V. Tran, T. D. Le, G. L. Bach, and L. D. Tran, "Studying Ni (II) adsorption of magnetite/graphene oxide/chitosan nanocomposite," *Advances in Polymer Technology*, vol. 2019, Article ID 8124351, 2019.

[36] H. V. Tran, A. X. Trinh, C. D. Huynh, and H. Q. Le, "Facile hydrothermal synthesis of silver/chitosan nanocomposite and application in the electrochemical detection of hydrogen peroxide," *Sensor Letters*, vol. 14, pp. 32–38, 2016.

[37] H.-M. Ju, S.-H. Choi, and S. H. Huh, "X-ray diffraction patterns of thermally-reduced graphenes," *Journal of the Korean Physical Society*, vol. 57, no. 6, p. 1649, 2010.

[38] Y. Du, M. Pei, Y. He, F. Yu, W. Guo, and L. Wang, "Preparation, characterization and application of magnetic Fe3O4-CS for the adsorption of orange I from aqueous solutions," *PLoS One*, vol. 9, no. 10, article e108647, 2014.

[39] M. Liu, T. Wen, X. Wu et al., "Synthesis of porous Fe3O4 hollow microspheres/graphene oxide composite for Cr(VI) removal," *Dalton Transactions*, vol. 42, no. 41, pp. 14710–14717, 2013.

[40] S. ul Haque, A. Nasar, and M. M. R. Inamuddin, "Applications of chitosan (CHI)-reduced graphene oxide (rGO)-polyaniline (PAni) conducting composite electrode for energy generation in glucose biofuel cell," *Scientific Reports*, vol. 10, article 10428, 2020.

[41] M. Yadav, Y. Y. Rhee, S. J. Park, and D. Hui, "Mechanical properties of Fe3O4/GO/chitosan composites," *Composites Part B: Engineering*, vol. 66, pp. 89–96, 2014.

[42] X. Rong, F. Qiu, C. Zhang, L. Fu, Y. Wang, and D. Yang, "Adsorption–photodegradation synergetic removal of methylene blue from aqueous solution by NiO/graphene oxide nanocomposite," *Powder Technology*, vol. 275, pp. 322–328, 2015.

[43] Y. Yang, Y. Xie, L. Pang et al., "Preparation of reduced graphene oxide/poly(acrylamide) nanocomposite and its adsorption of Pb(II) and methylene blue," *Langmuir*, vol. 29, pp. 10727–10736, 2013.

[44] H. C. Vu, A. D. Dwivedi, T. T. Le, S.-H. Seo, E.-J. Kim, and Y.-S. Chang, "Magnetite graphene oxide encapsulated in alginate beads for enhanced adsorption of Cr(VI) and As(V) from aqueous solutions: role of crosslinking metal cations in pH control," *Chemical Engineering Journal*, vol. 307, pp. 220–229, 2017.

[45] N. T. Nguyen, N. T. Nguyen, and V. A. Nguyen, "In situ synthesis and characterization of ZnO/chitosan nanocomposite as an adsorbent for removal of Congo red from aqueous solution," *Advances in Polymer Technology*, vol. 2020, Article ID 3892694, 2020.

[46] H. Shi, J. Yang, L. Zhu et al., "Removal of Pb^{2+}, Hg^{2+}, and Cu^{2+} by chain-like Fe_3O_4@SiO_2@chitosan magnetic nanoparticles," *Journal of Nanoscience and Nanotechnology*, vol. 16, pp. 1871–1882, 2016.

[47] H. V. Tran, H. V. Nguyen, D. V. Vu, T. D. Le, B. T. Nguyen, and D. H. Le, "Carbon coated MFe_2O_4 (M=Fe, Co, Ni) magnetite nanoparticles: a smart adsorbent for direct yellow and moderacid red dyes," *Korean Journal of Chemical Engineering*, 2021.

[48] S. Thangavel, S. Thangavel, N. Raghavan, K. Krishnamoorthy, and G. Venugopal, "Visible-light driven photocatalytic degradation of methylene-violet by rGO/Fe_3O_4/ZnO ternary nanohybrid structures," *Journal of Alloys and Compounds*, vol. 665, pp. 107–112, 2016.

[49] A. A. Al-Kahtani and M. F. A. Taleb, "Photocatalytic degradation of Maxilon C.I. basic dye using CS/$CoFe_2O_4$/GONCs as a heterogeneous photo-Fenton catalyst prepared by gamma irradiation," *Journal of Hazardous Materials*, vol. 309, pp. 10–19, 2016.

[50] N. Song, X. L. Wu, S. Zhong, H. Lin, and J.-R. Chen, "Biocompatible G-Fe_3O_4/CA nanocomposites for the removal of methylene blue," *Journal of Molecular Liquids*, vol. 212, pp. 63–69, 2015.

[51] W. Zhu, X. Jiang, F. Liu, F. You, and C. Yao, "Preparation of chitosan—graphene oxide composite aerogel by hydrothermal method and its adsorption property of methyl orange," *Polymers*, vol. 12, no. 9, p. 2169, 2020.

[52] L. Fan, C. Luo, M. Sun, H. Qiu, and X. Li, "Synthesis of magnetic β-cyclodextrin–chitosan/graphene oxide as nanoadsorbent and its application in dye adsorption and removal," *Colloids and Surfaces B: Biointerfaces*, vol. 103, pp. 601–607, 2013.

[53] Z. Zhang and J. Kong, "Novel magnetic Fe_3O_4@ C nanoparticles as adsorbents for removal of organic dyes from aqueous solution," *Journal of Hazardous Materials*, vol. 193, pp. 325–329, 2011.

[54] R. Jiang, Y.-Q. Fu, H.-Y. Zhu, J. Yao, and L. Xiao, "Removal of methyl orange from aqueous solutions by magnetic maghemite/chitosan nanocomposite films: adsorption kinetics and equilibrium," *Journal of Applied Polymer Science*, vol. 125, no. S2, pp. E540–E549, 2012.

[55] W. Song, B. Gao, X. Xu et al., "Adsorption–desorption behavior of magnetic amine/Fe_3O_4 functionalized biopolymer resin towards anionic dyes from wastewater," *Bioresource Technology*, vol. 210, pp. 123–130, 2016.

[56] S. Ghorai, A. K. Sarkar, A. B. Panda, and S. Pal, "Effective removal of Congo red dye from aqueous solution using modified xanthan gum/silica hybrid nanocomposite as adsorbent," *Bioresource Technology*, vol. 144, pp. 485–491, 2013.

[57] J. Xu, D. Xu, B. Zhu, B. Cheng, and C. Jiang, "Adsorptive removal of an anionic dye Congo red by flower-like hierarchical magnesium oxide (MgO)-graphene oxide composite microspheres," *Applied Surface Science*, vol. 435, pp. 1136–1142, 2018.

[58] Y.-R. Zhang, P. Su, J. Huang, Q.-R. Wang, and B.-X. Zhao, "A magnetic nanomaterial modified with poly-lysine for efficient removal of anionic dyes from water," *Chemical Engineering Journal*, vol. 262, pp. 313–318, 2015.